Mechanism for resistive switching in chalcogenide-based electrochemical metallization memory cells

Fei Zhuge, Kang Li, Bing Fu, Hongliang Zhang, Jun Li, Hao Chen, Lingyan Liang, Junhua Gao, Hongtao Cao, Zhimin Liu, and Hao Luo

Citation: AIP Advances **5**, 057125 (2015); doi: 10.1063/1.4921089
View online: http://dx.doi.org/10.1063/1.4921089
View Table of Contents: http://scitation.aip.org/content/aip/journal/adva/5/5?ver=pdfcov
Published by the AIP Publishing

Articles you may be interested in

Mechanism for resistive switching in an oxide-based electrochemical metallization memory
Appl. Phys. Lett. **100**, 072101 (2012); 10.1063/1.3683523

Simulation of multilevel switching in electrochemical metallization memory cells
J. Appl. Phys. **111**, 014501 (2012); 10.1063/1.3673239

Metal oxide resistive memory switching mechanism based on conductive filament properties
J. Appl. Phys. **110**, 124518 (2011); 10.1063/1.3671565

Electrode kinetics of Cu – Si O 2 -based resistive switching cells: Overcoming the voltage-time dilemma of electrochemical metallization memories
Appl. Phys. Lett. **94**, 072109 (2009); 10.1063/1.3077310

Analytical model for subthreshold conduction and threshold switching in chalcogenide-based memory devices
J. Appl. Phys. **102**, 054517 (2007); 10.1063/1.2773688

computing in SCIENCE & ENGINEERING
AIP's JOURNAL OF COMPUTATIONAL TOOLS AND METHODS.
AVAILABLE AT MOST LIBRARIES.

All article content, except where otherwise noted, is licensed under a Creative Commons Attribution 3.0 Unported license. See: http://creativecommons.org/licenses/by/3.0/ Downloaded to IP: 210.72.19.250 On: Mon, 11 May 2015 00:39:22

AIP ADVANCES **5**, 057125 (2015)

Mechanism for resistive switching in chalcogenide-based electrochemical metallization memory cells

Fei Zhuge,[1,a] Kang Li,[1,2] Bing Fu,[1] Hongliang Zhang,[1] Jun Li,[1] Hao Chen,[1] Lingyan Liang,[1] Junhua Gao,[1] Hongtao Cao,[1,a] Zhimin Liu,[1] and Hao Luo[1]
[1]*Ningbo Institute of Materials Technology and Engineering, Chinese Academy of Sciences, Ningbo 315201, China*
[2]*Nano Science and Technology Institute, University of Science and Technology of China, Suzhou 215123, China*

(Received 9 March 2015; accepted 3 May 2015; published online 8 May 2015)

It has been reported that in chalcogenide-based electrochemical metallization (ECM) memory cells (e.g., As_2S_3:Ag, GeS:Cu, and Ag_2S), the metal filament grows from the cathode (e.g., Pt and W) towards the anode (e.g., Cu and Ag), whereas filament growth along the opposite direction has been observed in oxide-based ECM cells (e.g., ZnO, ZrO_2, and SiO_2). The growth direction difference has been ascribed to a high ion diffusion coefficient in chalcogenides in comparison with oxides. In this paper, upon analysis of OFF state *I–V* characteristics of ZnS-based ECM cells, we find that the metal filament grows from the anode towards the cathode and the filament rupture and rejuvenation occur at the cathodic interface, similar to the case of oxide-based ECM cells. It is inferred that in ECM cells based on the chalcogenides such as As_2S_3:Ag, GeS:Cu, and Ag_2S, the filament growth from the cathode towards the anode is due to the existence of an abundance of ready-made mobile metal ions in the chalcogenides rather than to the high ion diffusion coefficient. *© 2015 Author(s). All article content, except where otherwise noted, is licensed under a Creative Commons Attribution 3.0 Unported License.* [http://dx.doi.org/10.1063/1.4921089]

I. INTRODUCTION

Electrochemical metallization (ECM) memory cells, based on Ag or Cu ion migration-induced resistive switching (RS), has attracted increasing attention due to its superior advantages of simple structure, super-high density, high operation speed, and compatibility with the complementary metal oxide semiconductor (CMOS) process.[1,2] The ECM cell consists of an insulator layer sandwiched between two electrodes, in which one is made from an electrochemically active electrode (AE) metal, such as Ag or Cu, and the other is a counter electrode (CE), such as Pt, Ir, W, or Ag.[3,4] Till now, a large number of ECM cells have been reported, employing various insulating materials such as chalcogenides,[5–13] oxides,[14–24] amorphous Si (Refs. 25 and 26) and C,[27–30] and organic materials.[31,32]

For the RS mechanism of ECM cells, the most widely accepted hypothesis is as follows,[1–3] with Cu as the AE (anode) and Pt as the CE (cathode) metal: (i) anodic dissolution of Cu; (ii) drift of the Cu ions across the insulator film; (iii) reduction and electro-crystallization of Cu on the CE surface, leading to the formation of a conical filament with the base and the tip located at the cathodic and the anodic interfaces, and switching the cell ON; (iv) electrochemical dissolution at the weakest point along the length of the filament, i.e., near the anodic interface as a sufficient opposite polarity voltage is applied, switching the cell OFF. Steps (i)–(iii) represent the "Forming" or "SET" process, whereas step (iv) is the "RESET" process. The formation/rupture of metal filaments have been directly observed in chalcogenide-based ECM cells (e.g., Ag/As_2S_3:Ag/Au,[33]

[a]Authors to whom correspondence should be addressed. Electronic addresses: zhugefei@nimte.ac.cn. and h_cao@nimte.ac.cn.

 ©Author(s) 2015

All article content, except where otherwise noted, is licensed under a Creative Commons Attribution 3.0 Unported license. See: http://creativecommons.org/licenses/by/3.0/ Downloaded to IP: 210.72.19.250 On: Mon, 11 May 2015 00:39:22

Ag/GeSe:Ag/Ni,[34] Pt:Ir/GeS:Cu/Pt:Ir,[35] and Ag/Ag_2S/W (Ref. 36)), providing direct evidence to this hypothesis. However, in our previous work,[37] a different filament growth mode has been proposed for Cu/ZnO/Pt ECM cells, i.e., the filament grows from the AE (Cu) towards the CE (Pt), and the filament rupture and rejuvenation occur at the cathodic interface. More importantly, metal filament growth corresponding to this mode has been directly observed in oxide-based ECM cells (e.g., Cu/ZrO_2/Pt,[38] Ag/SiO_2/Pt,[39,40] Ag/SiO_2/W,[17] and Ag/SiO_2/p^+-Si (Ref. 41)). The filament growth mode variance has been attributed to a low ion diffusion coefficient in oxides in comparison with sulfides and selenides.

In this work, we study the RS mechanism of ZnS-based ECM cells. Surprisingly, the results reveal that in such sulfide-based devices, the metal filament rupture/rejuvenation occurs at the cathodic interface, and thus the filament very likely grows from the anode towards the cathode, similar to the case of oxide-based ECM cells. This study suggests that in As_2S_3:Ag-,[33] GeSe:Ag-,[34] GeS:Cu-,[35] and Ag_2S-based (Ref. 36) ECM cells, the filament growth from the cathode towards the anode is due to the existence of an abundance of ready-made mobile metal ions in the chalcogenides rather than to the high ion diffusion coefficient.

II. EXPERIMENT

ZnS thin films with a thickness of ~100 nm were deposited on Pt/Ti/SiO_2/Si and ITO (In_2O_3:Sn, resistivity ~10^{-4} Ω cm) coated glass substrates at room temperature (RT) by rf magnetron sputtering in Ar ambient using a ceramic ZnS target. The ZnS film structure was examined by X-ray diffraction (XRD). Cu top electrodes (AE or anode) with a diameter of 30 and 100 μm were deposited on ZnS films at RT by electron-beam evaporation. The cells with 100 μm top electrodes were used for I–V measurement, whereas the cells with 30 μm top electrodes for conducting atomic force microscopy (CAFM) measurement. I–V characteristics of the Cu/ZnS/Pt and Cu/ZnS/ITO ECM cells were measured at RT in air using a Keithley 4200 semiconductor parameter analyzer. During the measurement, the positive bias was defined as the current flowing from the top to the bottom (CE or cathode) electrode, and vise versa. Before the CAFM measurement, the cells underwent an Electroforming process followed by removing the Cu electrodes using adhesive tape.

III. RESULTS AND DISCUSSION

The XRD pattern of ZnS thin films presents a weak diffraction peak at $2\theta = 28.7°$ corresponding to cubic (111) or hexagonal (002) reflection of ZnS. Given that low temperature growth of ZnS results in the cubic structure,[42,43] this peak can be assigned to cubic ZnS (111) plane. The XRD pattern indicates that the as-grown ZnS has a polycrystalline structure. Given that Cu/$(ZnS)_{0.8}(SiO_2)_{0.2}$/TiW (Ref. 44) and Cu/$Zn_{0.3}Cd_{0.7}S$/Pt (Ref. 8) sandwiches have been reported to exhibit bipolar RS resulting from the formation/rupture of Cu filaments, it could be reasonably deduced that a similar RS mechanism will work in our ZnS-based devices. The Electroforming voltages of the Cu/ZnS/Pt and Cu/ZnS/ITO cells are ~1.3 and ~2 V, respectively.

Figures 1(a) and 1(b) show the AFM and CAFM images for Cu/ZnS/Pt after the Electroforming operation, respectively. Before the measurement, the Cu top electrode was removed by adhesive tape. Nearly all the Cu has been dislodged from the ZnS film surface except a small spike as marked by the blue arrow (Fig. 1(a)), where an abrupt current increase is observed correspondingly (Fig. 1(b)). The small spike is speculated to be Cu coming from the electrode since it is highly conductive. As we know, once a complete Cu filament forms, a high current flows through the filament inducing large amounts of Joule heat which significantly accelerates the inter-diffusion of Cu atoms at the filament/electrode interface. It is similar to a welding process thus resulting in incomplete separation of the filament and the electrode. Note that after removing the Cu electrode, bulges can be clearly observed around the edge of the region previously occupied by the electrode (Fig. 1(a)). It has been reported that compared to the central area of the Cu electrode, the margin of the Cu electrode is apt to be oxidized to $Cu(OH)_2$ in air.[45] Therefore, the bulges are likely dominated by $Cu(OH)_2$ which is difficult to be removed by adhesive tape compared to Cu. We can thus conclude that only a single complete Cu filament forms after the Electroforming operation for Cu/ZnS/Pt ECM cells.

All article content, except where otherwise noted, is licensed under a Creative Commons Attribution 3.0 Unported license. See: http://creativecommons.org/licenses/by/3.0/ Downloaded to IP: 210.72.19.250 On: Mon, 11 May 2015 00:39:22

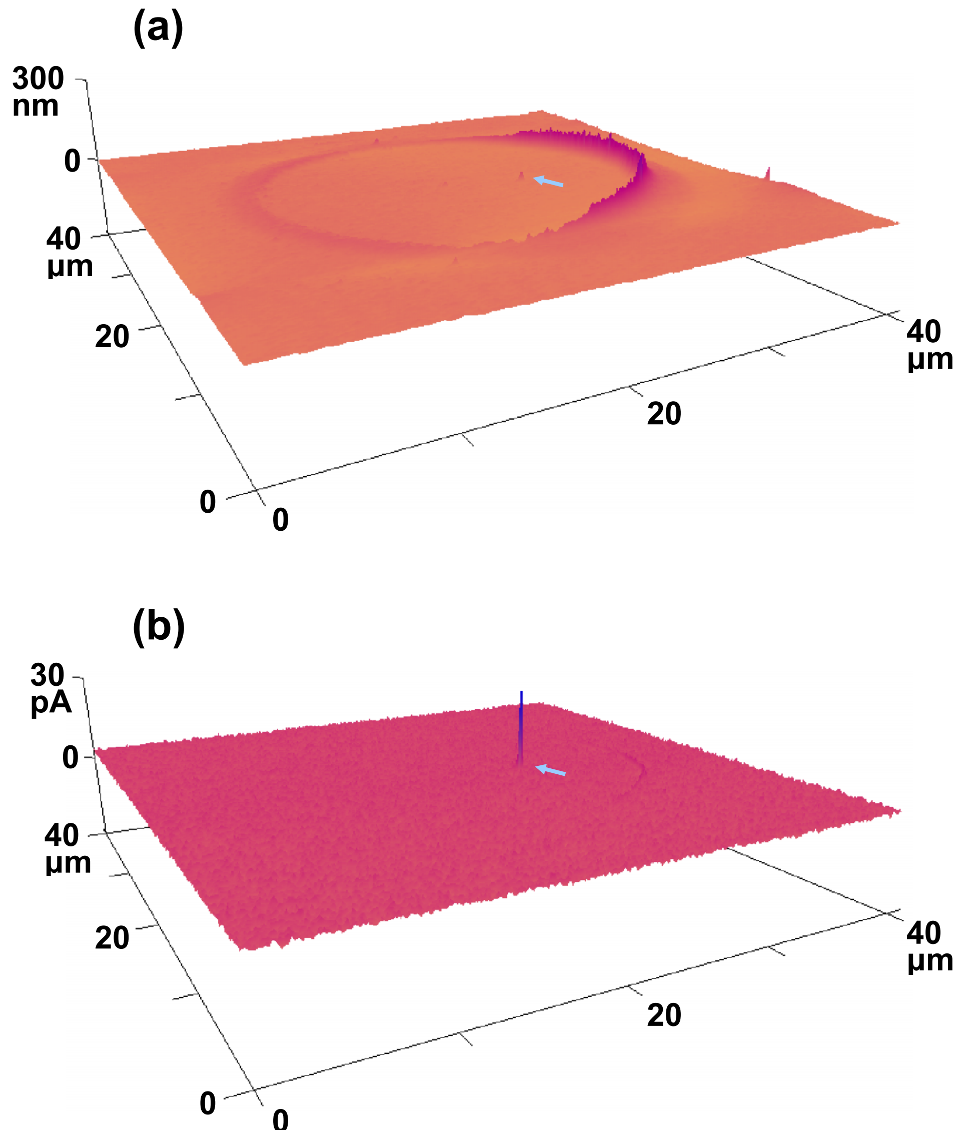

FIG. 1. (a) AFM and (b) CAFM images for Cu/ZnS/Pt after the Electroforming operation. The Cu top electrode was removed by adhesive tape. A low voltage of 50 mV was used to prevent resistance state change of the sample. The blue arrows show the position where the surface morphology and current change abruptly.

Figures 2(a) and 2(c) present the typical *I*–*V* characteristics of the RESET (ON-to-OFF switching) and subsequent SET (OFF-to-ON switching) processes for Cu/ZnS/Pt and Cu/ZnS/ITO ECM cells, respectively. Both cells show bipolar RS behavior. Figures 2(b) and 2(d) highlight the OFF state *I*–*V* curves of Cu/ZnS/Pt and Cu/ZnS/ITO, respectively. The important feature of Figs. 2(b) and 2(d) is the asymmetry of both *I*–*V* curves with respect to the bias voltage. We see that for Cu/ZnS/Pt, the current demonstrates a clear rectifying effect with a higher current value in the negative voltage branch, whereas in the case of Cu/ZnS/ITO, the circumstance is just the reverse. Since Joule heating plays an important role in the RESET, ECM cells can also be operated in the unipolar RS mode although the endurance is very poor.[46,47] Figure 3 shows the *I*–*V* characteristics of the unipolar RS and corresponding OFF state *I*–*V* asymmetry for both cells. The asymmetry is found to be similar to that in the bipolar RS mode. For both cells operated in the bipolar or unipolar mode, the ON/OFF current ratio varies in a wide range from 10 to $\sim 10^8$.

To interpret the OFF state *I*–*V* asymmetry variance between Cu/ZnS/Pt and Cu/ZnS/ITO, we first need to discuss the ideal *I*–*V* of the various possible OFF states of the ECM cells. It is always

All article content, except where otherwise noted, is licensed under a Creative Commons Attribution 3.0 Unported license. See: http://creativecommons.org/licenses/by/3.0/ Downloaded to IP: 210.72.19.250 On: Mon, 11 May 2015 00:39:22

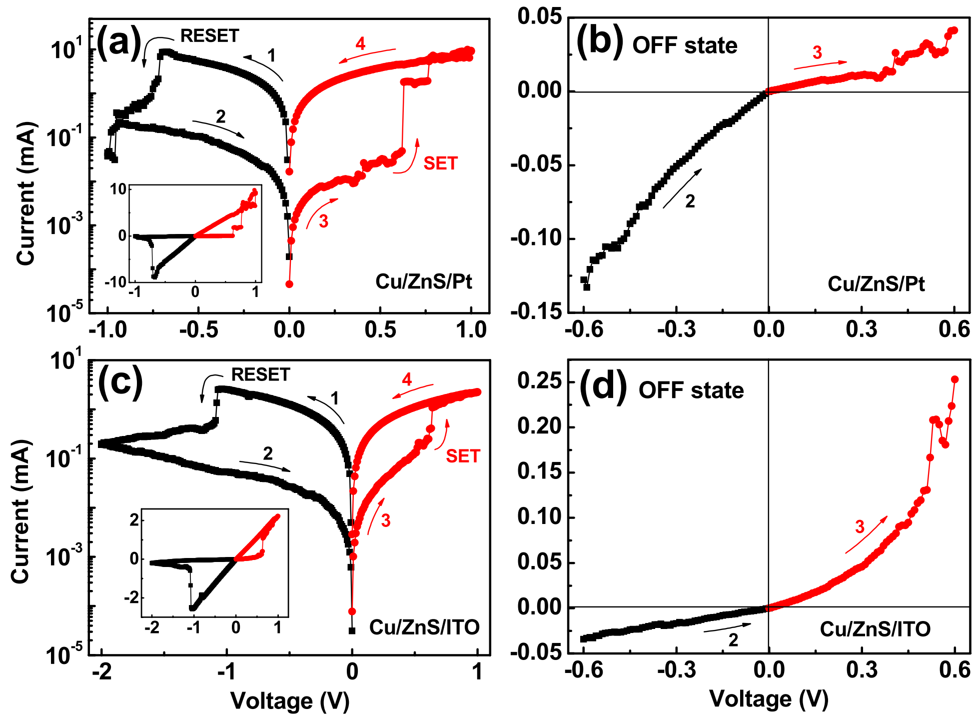

FIG. 2. Typical I–V characteristics of the RESET and subsequent SET processes for (a) Cu/ZnS/Pt and (c) Cu/ZnS/ITO ECM cells. The insets show the curves on a linear scale. (b) and (d) highlight the corresponding OFF state curves.

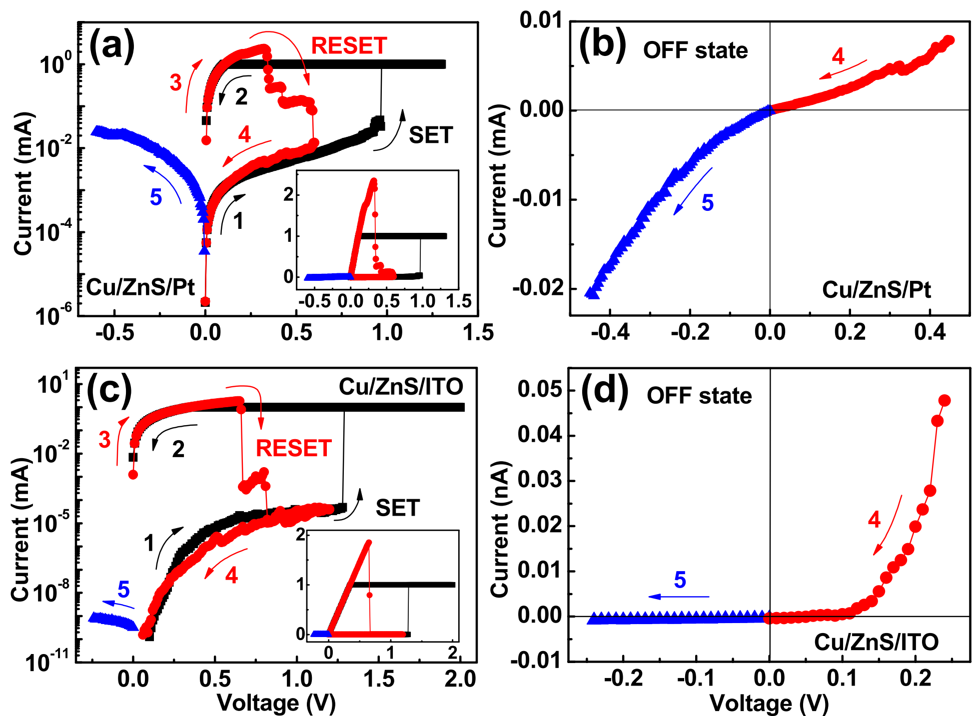

FIG. 3. Typical I–V characteristics of the unipolar RS for (a) Cu/ZnS/Pt and (c) Cu/ZnS/ITO ECM cells. The insets show the curves on a linear scale. (b) and (d) highlight the corresponding OFF state curves. To study the OFF state I–V asymmetry, the I–V characteristics in the negative voltage branch were also measured after the cells were RESET to the OFF state (step 5).

All article content, except where otherwise noted, is licensed under a Creative Commons Attribution 3.0 Unported license. See: http://creativecommons.org/licenses/by/3.0/ Downloaded to IP: 210.72.19.250 On: Mon, 11 May 2015 00:39:22

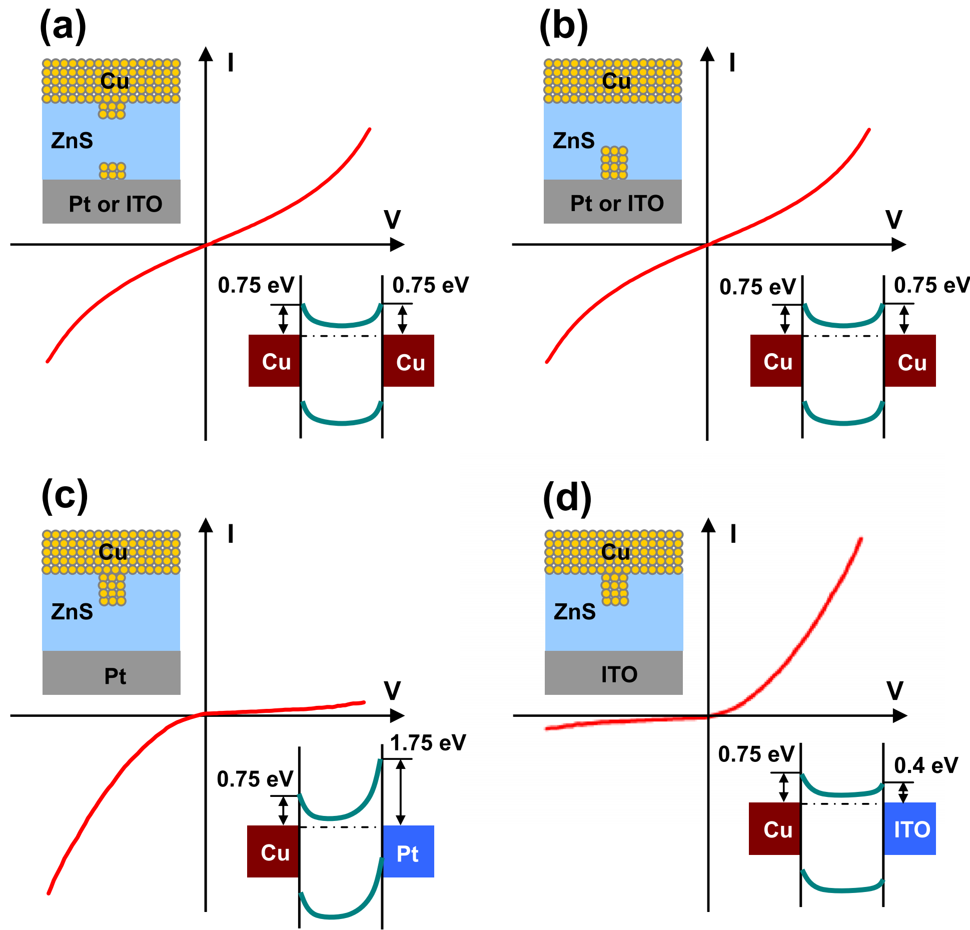

FIG. 4. Schematic ideal *I–V* characteristics of three possible OFF states of Cu/ZnS/Pt (or ITO) ECM cells. The insets schematically illustrate three possible OFF states and the corresponding band diagrams of the insulating gaps (i.e., ZnS) sandwiched between two Cu filament segments (a), Cu electrode and Cu filament (b), and Cu filament and Pt (c) or ITO (d) electrode.

considered that the conducting filament rupture/rejuvenation occurs at a localized position.[1–3] The *I–V* characteristics of three possible OFF states of Cu/ZnS/Pt (or ITO) cells are schematically illustrated in Fig. 4. In the OFF state, *I–V* characteristics are governed by the insulating gap (ZnS) sandwiched between the electrode and the remaining metal filament (Figs. 4(b)–3(d)) or two filament segments (Fig. 4(a)). As shown in Figs. 4(a) and 4(b), the Cu/gap/Cu structures consist of two back-to-back symmetric Schottky barriers (SBs) at Cu/gap junctions, inducing symmetric *I–V* curves with respect to the bias voltage. As for Cu/gap/Pt, the band structure is asymmetric due to different SB heights of Cu/ZnS (~0.75 eV) and ZnS/Pt (~1.75 eV), as schematically illustrated in the inset of Fig. 4(c). Herein, the SB heights are estimated from the differences between the electron affinity of ZnS (~3.9 eV) and the work functions of electrode metals (4.65 eV for Cu and 5.65 eV for Pt).[48] When a bias voltage is applied, one SB is under reverse bias, while the other is forward biased simultaneously. The whole impedance is always dominated by the reverse-biased SB.[49] For Cu/gap/Pt, the impedance is determined by the ZnS/Pt SB at a positive bias; while at a negative bias, the impedance is determined by the Cu/ZnS SB. The different SB heights result in a rectifying *I–V* curve with a higher current value in the negative voltage branch, as shown in Fig. 4(c). While in the case of Cu/gap/ITO, the asymmetric band structure results from different SB heights of Cu/ZnS (~0.75 eV) and ZnS/ITO (~0.4 eV), as schematically shown in the inset of Fig. 4(d). Herein, the SB height of ZnS/ITO is estimated from the difference between the electron affinity of ZnS and the

All article content, except where otherwise noted, is licensed under a Creative Commons Attribution 3.0 Unported license. See: http://creativecommons.org/licenses/by/3.0/ Downloaded to IP: 210.72.19.250 On: Mon, 11 May 2015 00:39:22

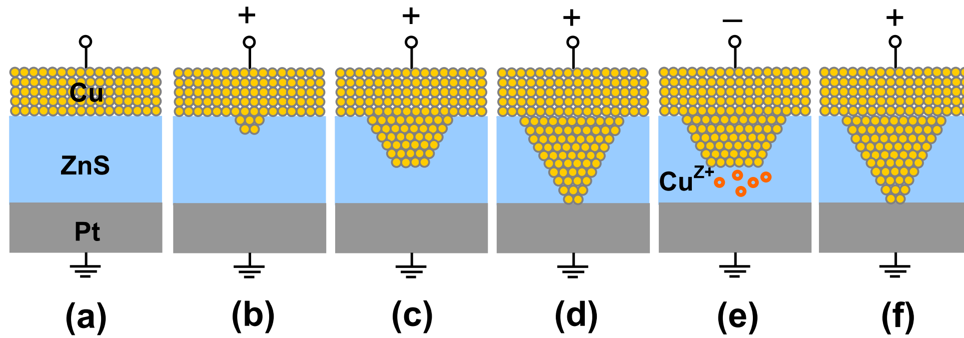

FIG. 5. Schematic (a) pristine state, (b)–(d) Electroforming process, (e) RESET process, and (f) SET process of Cu/ZnS/Pt ECM cells. Cu^{Z+} represents copper ions, where Z = 1 or 2.

work function of ITO (~4.3 eV for ITO cleaned by Ar ion sputtering).[50] The impedance is determined by the ZnS/ITO SB at a positive bias; while at a negative bias, the impedance is determined by the Cu/ZnS SB. The different SB heights result in a rectifying *I–V* curve with a higher current value in the positive voltage branch, as shown in Fig. 4(d).

By comparing *I–V* characteristics shown in Figs. 2, 3, and 4, it can be reasonably concluded that the rupture and rejuvenation of Cu filament occur at the ZnS/Pt (or ITO) interface. Given that the filament is apt to be ruptured at the weakest position along its length,[1–3,51] it very likely has a conical shape, with the base and the tip located at the anodic (AE, Cu) and the cathodic (CE, Pt or ITO) interfaces, respectively. It follows that the filament is most likely to grow from the anode towards the cathode. The complete filament formation process (i.e., Electroforming) is schematically illustrated in Figs. 5(b)–5(d). The subsequent schematic RESET and SET processes are shown in Figs. 5(e) and 5(f), respectively. For the RESET process with a negative (or positive) bias voltage applied to the AE, the filament near the cathodic interface is dissolved by Joule heating assisted electrochemical reactions, switching the device OFF. The following SET process only needs to rejuvenate the previously ruptured filament segment, giving rise to a lower SET voltage compared to the Electroforming process.[37] The inferred growth direction of Cu filament in Cu/ZnS/Pt is similar to that in oxide-based ECM cells.[17,37–41] The formation of the Cu filament may result from the bipolar electrochemical mass transfer of Cu nanoclusters in ZnS.[17,41]

As mentioned previously, the As_2S_3:Ag-,[33] GeSe:Ag-,[34] GeS:Cu-,[35] and Ag_2S-based (Ref. 36) ECM cells show metal filament growth with a direction from the cathode towards the anode, totally opposite to the filament growth direction in ZnS-based ECM cells. It is unlikely that such filament growth direction variance is attributed to a difference in ion diffusion coefficient. The important feature of As_2S_3:Ag *etc.* is that these chalcogenides themselves contain a large number of ready-made movable Cu or Ag ions. Figure 6 schematically presents the overall RS process for

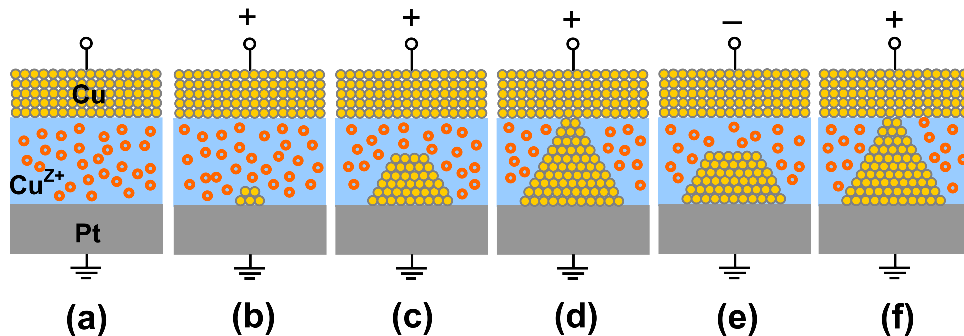

FIG. 6. Schematic (a) pristine state, (b)–(d) Electroforming process, (e) RESET process, and (f) SET process of Cu/chalcogenide/Pt ECM cells, where the chalcogenide itself contains an abundance of ready-made movable Cu ions (Cu^{Z+}, Z = 1 or 2).

All article content, except where otherwise noted, is licensed under a Creative Commons Attribution 3.0 Unported license. See: http://creativecommons.org/licenses/by/3.0/ Downloaded to IP: 210.72.19.250 On: Mon, 11 May 2015 00:39:22

such chalcogenide-based ECM cells, with Cu as the anode metal and dopant and Pt as the cathode metal. As applying an appropriate positive voltage to the anode, Cu ions in the electrolyte will drift towards the cathode. Owing to an abundant quantity as well as a short migration distance, the ions near the cathode will get to this electron-supplying electrode rapidly and then be reduced to Cu atoms by capturing electrons. As the Cu concentration approaches supersaturation, inhomogeneous nucleation occurs (see Fig. 6(b)).[46] The nucleus grows forward by harvesting ions until touching the anode, as illustrated in Figs. 6(c) and 6(d). At the same time, to maintain charge neutrality, Cu ions are injected into the chalcogenide via oxidation at the anode.[52] The subsequent RESET and SET will occur at Cu/chalcogenide interface, as illustrated in Figs. 6(e) and 6(f). Based on the discussion above, we can conclude that in As_2S_3:Ag-,[33] GeSe:Ag-,[34] GeS:Cu-,[35] and Ag_2S-based (Ref. 36) ECM cells, the opposite filament growth direction (from the cathode towards the anode) should be due to the existence of a large number of ready-made movable Ag or Cu ions in the chalcogenides rather than to a high ion diffusion coefficient.[37]

IV. CONCLUSIONS

We have investigated the different asymmetry of *I–V* characteristics in the OFF state of Cu/ZnS/Pt and Cu/ZnS/ITO ECM cells. The results indicate that the Cu filament rupture and rejuvenation occur at the ZnS/Pt (or ITO) interface, i.e., the cathodic interface. The filament most likely has a conical shape, with the base and the tip located at the anodic and the cathodic interfaces, respectively. It follows that the filament is likely to grow from the anode towards the cathode, much different from the case of chalcogenide-based ECM cells where the chalcogenides (e.g., As_2S_3:Ag,[33] GeSe:Ag,[34] GeS:Cu,[35] and Ag_2S (Ref. 36)) contain an abundance of ready-made mobile cations, i.e., Cu or Ag ions.

ACKNOWLEDGMENTS

We would like to thank Prof. Ping Cui for her kind help in our preparation of this paper. This work was supported by National Natural Science Foundation of China (Nos. 51272261 and 61474127), Chinese National Program on Key Basic Research Project (No. 2012CB933003), Zhejiang (No. LR15F040002) and Ningbo Natural Science Foundations.

[1] F. Pan, S. Gao, C. Chen, C. Song, and F. Zeng, Mat. Sci. Eng. R **83**, 1 (2014).
[2] I. Valov, R. Waser, J. R. Jameson, and M. N. Kozicki, Nanotechnology **22**, 254003 (2011).
[3] R. Waser, R. Dittmann, G. Staikov, and K. Szot, Adv. Mater. **21**, 2632 (2009).
[4] X. Guo, C. Schindler, S. Menzel, and R. Waser, Appl. Phys. Lett. **91**, 133513 (2007).
[5] R. Symanczyk, R. Bruchhaus, R. Dittrich, and M. Kund, IEEE Electron Device Lett. **30**, 876 (2009).
[6] C. Gopalan, Y. Ma, T. Gallo, J. Wang, E. Runnion, J. Saenz, F. Koushan, P. Blanchard, and S. Hollmer, Solid State Electron. **58**, 54 (2011).
[7] D. Kamalanathan, U. Russo, D. Ielmini, and M. N. Kozicki, IEEE Electron Device Lett. **30**, 553 (2009).
[8] Z. Wang, P. B. Griffin, J. McVittie, S. Wong, P. C. McIntyre, and Y. Nishi, IEEE Electron Device Lett. **28**, 14 (2007).
[9] H. X. Guo, L. G. Gao, Y. D. Xia, K. Jiang, B. Xu, Z. G. Liu, and J. Yin, Appl. Phys. Lett. **94**, 153504 (2009).
[10] R. Bruchhaus, M. Honal, R. Symanczyk, and M. Kund, J. Electrochem. Soc. **156**, H729 (2009).
[11] M. Kund, G. Beitel, C. U. Pinnow, T. Roehr, J. Schumann, R. Symanczyk, K. D. Ufert, and G. Mueller, Tech. Dig. – Int. Electron Devices Meet. **2005**, 754.
[12] N. E. Gilbert and M. N. Kozicki, IEEE J. Solid-State Circuits **42**, 1383 (2007).
[13] L. Chen, Z. G. Liu, Y. D. Xia, K. B. Yin, L. G. Gao, and J. Yin, Appl. Phys. Lett. **94**, 162112 (2009).
[14] Y. C. Yang, F. Pan, Q. Liu, M. Liu, and F. Zeng, Nano Lett. **9**, 1636 (2009).
[15] F. Zhuge, S. S. Peng, C. L. He, X. J. Zhu, X. X. Chen, Y. W. Liu, and R. W. Li, Nanotechnology **22**, 275204 (2011).
[16] L. Shi, D. S. Shang, J. R. Sun, and B. G. Shen, Phys. Status Solidi RRL **4**, 344 (2010).
[17] Y. C. Yang, P. Gao, L. Z. Li, X. Q. Pan, S. Tappertzhofen, S. H. Choi, R. Waser, I. Valov, and W. D. Lu, Nat. Commun. **5**, 4232 (2014).
[18] M. N. Kozicki, C. Gopalan, M. Balakrishnan, and M. Mitkova, IEEE Trans. Nanotechnol. **5**, 535 (2006).
[19] C. Schindler, G. Staikov, and R. Waser, Appl. Phys. Lett. **94**, 072109 (2009).
[20] S. C. Puthentheradam, D. K. Schroder, and M. N. Kozicki, Appl. Phys. A **102**, 817 (2011).
[21] T. Sakamoto, N. Banno, N. Iguchi, H. Kawaura, H. Sunamura, S. Fujieda, K. Terabe, T. Hasegawa, and M. Aono, Dig. Tech. Pap. - Symp. VLSI Technol. **2007**, 38.
[22] K. Tsunoda, Y. Fukuzumi, J. R. Jameson, Z. Wang, P. B. Griffin, and Y. Nishi, Appl. Phys. Lett. **90**, 113501 (2007).
[23] Q. Liu, C. M. Dou, Y. Wang, S. B. Long, W. Wang, M. Liu, M. H. Zhang, and J. N. Chen, Appl. Phys. Lett. **95**, 023501 (2009).

All article content, except where otherwise noted, is licensed under a Creative Commons Attribution 3.0 Unported license. See: http://creativecommons.org/licenses/by/3.0/ Downloaded to IP: 210.72.19.250 On: Mon, 11 May 2015 00:39:22

[24] T. Kever, U. Bottger, C. Schindler, and R. Waser, Appl. Phys. Lett. **91**, 083506 (2007).
[25] X. B. Yan, Y. F. Chen, H. Hao, Q. Liu, E. P. Zhang, S. S. Shi, and J. Z. Lou, Appl. Phys. Lett. **105**, 072104 (2014).
[26] S. H. Jo and W. Lu, Nano Lett. **8**, 392 (2008).
[27] H. Chen, F. Zhuge, B. Fu, J. Li, J. Wang, W. G. Wang, Q. Wang, L. Li, F. G. Li, H. L. Zhang, L. Y. Liang, H. Luo, M. Wang, J. H. Gao, H. T. Cao, H. Zhang, and Z. C. Li, Carbon **76**, 459 (2014).
[28] Y. Chai, Y. Wu, K. Takei, H. Y. Chen, S. M. Yu, P. C. H. Chan, A. Javey, and H. S. P. Wong, IEEE Trans. Electron Devices **58**, 3933 (2011).
[29] M. Pyun, H. Choi, J. B. Park, D. Lee, M. Hasan, R. Dong, S. J. Jung, J. Lee, D. Seong, J. Yoon, and H. Hwang, Appl. Phys. Lett. **93**, 212907 (2008).
[30] F. Zhuge, J. Li, H. Chen, J. Wang, L. Q. Zhu, B. R. Bian, B. Fu, Q. Wang, L. Li, R. B. Pan, L. Y. Liang, H. L. Zhang, H. T. Cao, H. Zhang, Z. C. Li, J. H. Gao, and K. Li, Appl. Phys. Lett. **106**, 083104 (2015).
[31] B. Cho, J. M. Yun, S. Song, Y. Ji, D. Y. Kim, and T. Lee, Adv. Funct. Mater. **21**, 3976 (2011).
[32] S. Z. Li, F. Zeng, C. Chen, H. Y. Liu, G. S. Tang, S. Gao, C. Song, Y. S. Lin, F. Pan, and D. Guo, J. Mater. Chem. C **1**, 5292 (2013).
[33] Y. Hirose and H. Hirose, J. Appl. Phys. **47**, 2767 (1976).
[34] M. N. Kozicki and M. Mitkova, J. Non-Cryst. Solids **352**, 567 (2006).
[35] T. Fujii, M. Arita, Y. Takahashi, and I. Fujiwara, Appl. Phys. Lett. **98**, 212104 (2011).
[36] Z. Xu, Y. Bando, W. L. Wang, X. D. Bai, and D. Golberg, ACS Nano **5**, 2515 (2010).
[37] S. S. Peng, F. Zhuge, X. X. Chen, X. J. Zhu, B. L. Hu, L. Pan, B. Chen, and R. W. Li, Appl. Phys. Lett. **100**, 072101 (2012).
[38] Q. Liu, J. Sun, H. B. Lv, S. B. Long, K. B. Yin, N. Wan, Y. T. Li, L. T. Sun, and M. Liu, Adv. Mater. **24**, 1844 (2012).
[39] Y. C. Yang, P. Gao, S. Gaba, T. Chang, X. Q. Pan, and W. Lu, Nat. Commun. **3**, 732 (2012).
[40] H. T. Sun, Q. Liu, C. F. Li, S. B. Long, H. B. Lv, C. Bi, Z. L. Huo, L. Li, and M. Liu, Adv. Funct. Mater. **24**, 5679 (2014).
[41] X. Z. Tian, S. Z. Yang, M. Zeng, L. F. Wang, J. K. Wei, Z. Xu, W. L. Wang, and X. D. Bai, Adv. Mater. **26**, 3649 (2014).
[42] V. L. Gayou, B. Salazar-Hernandez, M. E. Constantino, E. R. Andres, T. Diaz, R. D. Macuil, and M. R. Lopez, Vacuum **84**, 1191 (2010).
[43] D. H. Hwang, J. H. Ahn, K. N. Hui, K. S. Hui, and Y. G. Son, Nanoscale Res. Lett. **7**, 26 (2012).
[44] J. Q. Huang, L. P. Shi, E. G. Yeo, K. J. Yi, and R. Zhao, IEEE Electron Device Lett. **33**, 98 (2012).
[45] L. Y. Liang, H. T. Cao, Q. Liu, K. M. Jiang, Z. M. Liu, F. Zhuge, and F. L. Deng, ACS Appl. Mater. Interfaces **6**, 2255 (2014).
[46] T. Tsuruoka, K. Terabe, T. Hasegawa, and M. Aono, Nanotechnology **21**, 425205 (2010).
[47] W. H. Guan, M. Liu, S. B. Long, Q. Liu, and W. Wang, Appl. Phys. Lett. **93**, 223506 (2008).
[48] S. Kundu and L. C. Olsen, Thin Solid Films **471**, 298 (2005).
[49] X. S. Wu, M. Sprinkle, X. B. Li, F. Ming, C. Berger, and W. A. de Heer, Phys. Rev. Lett. **101**, 026801 (2008).
[50] K. Sugiyama, H. Ishii, Y. Ouchi, and K. Seki, J. Appl. Phys. **87**, 295 (2000).
[51] K. M. Kim, D. S. Jeong, and C. S. Hwang, Nanotechnology **22**, 254002 (2011).
[52] M. N. Kozicki, M. Balakrishnan, C. Gopalan, C. Ratnakumar, and M. Mitkova, Non-Volatile Memory Technol. Symp. Proc. **2005**, 83 (2005).

All article content, except where otherwise noted, is licensed under a Creative Commons Attribution 3.0 Unported license. See: http://creativecommons.org/licenses/by/3.0/ Downloaded to IP: 210.72.19.250 On: Mon, 11 May 2015 00:39:22